Article

Small Multivalent Architectures Mimicking Homotrimers of the TNF Superfamily Member CD40L: Delineating the Relationship between Structure and Effector Function

Nathalie Trouche, Sbastien Wieckowski, Weimin Sun, Olivier Chaloin, Johan Hoebeke, Sylvie Fournel, and Gilles Guichard

J. Am. Chem. Soc., **2007**, 129 (44), 13480-13492• DOI: 10.1021/ja073169m • Publication Date (Web): 13 October 2007

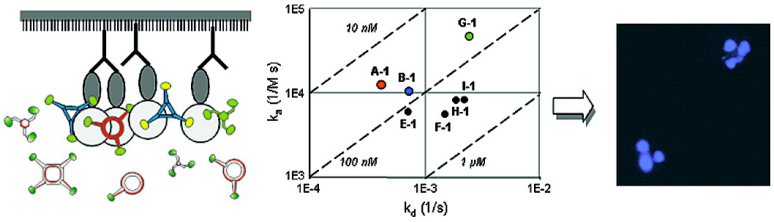

More About This Article

Additional resources and features associated with this article are available within the HTML version:

- Supporting Information
- Links to the 5 articles that cite this article, as of the time of this article download
- Access to high resolution figures
- Links to articles and content related to this article
- Copyright permission to reproduce figures and/or text from this article

View the Full Text HTML

J|A|C|S
ARTICLES
Published on Web 10/13/2007

Small Multivalent Architectures Mimicking Homotrimers of the TNF Superfamily Member CD40L: Delineating the Relationship between Structure and Effector Function

Nathalie Trouche,[†] Sébastien Wieckowski,[†] Weimin Sun,[†,‡] Olivier Chaloin,[†] Johan Hoebeke,[†] Sylvie Fournel,*[,†] and Gilles Guichard*[,†]

Contribution from the CNRS, Institut de Biologie Moléculaire et Cellulaire, laboratoire d'Immunologie et Chimie Thérapeutiques, 15 rue René Descartes, 67084 Strasbourg, France

Received May 4, 2007; E-mail: g.guichard@ibmc.u-strasbg.fr; s.fournel@ibmc.u-strasbg.fr

Abstract: Synthetic multivalent ligands, owing to the presence of multiple copies of a recognition motif attached to a central scaffold, can mediate clustering of cell surface receptors and thereby function as effector molecules. This paper dissects the relationship between structure and effector function of synthetic multivalent ligands targeting CD40, a cell surface receptor of the tumor necrosis factor receptor (TNF-R) superfamily. Triggering CD40 signaling *in vivo* can be used to enhance immunity against intracellular pathogens or tumors. A series of multimeric molecules has been prepared by systematically varying the shape and the valency of the *central scaffold*, the nature and the length of the *linker* as well as the sequence of the *receptor binding motif*. The data reported here (i) suggest that radial distribution of CD40-binding units and C_3-symmetry are preferred for optimal binding to CD40 and signaling, (ii) underscore the importance of choosing an appropriate linker to connect the receptor binding motif to the central scaffold, and (iii) show the versatility of planar cyclic α- and β-peptides as templates for the design of CD40L mimetics. In particular, the $(Ahx)_3$-**B** trimeric scaffold−linker combination equally accommodated binding elements derived from distinct CD40L hot-spot regions including AA″ loop and β-strand E. The use of *miniCD40Ls* such as those reported here is complementary to other approaches (recombinant ligands, agonistic anti-receptor antibodies) and may find interesting therapeutic applications. Furthermore, the results disclosed in this paper provide the basis for future design of other TNF family member mimetics.

Introduction

Protein−protein interactions are central to most biological processes from cellular communication to programmed cell death and provide the basis for interesting therapeutic applications. Small molecules that can bind at protein−protein interfaces are thus of interest to inhibit undesired biological processes or to promote desired ones.[1] The design of such molecules, however, is hampered by the large protein surfaces at interplay (1000−2000 Å^2 is generally considered as a "standard size" for the area buried in the interaction[2]), as well as by the difficulty to identify defined "hot spot" residues, and to handle conformational, nonsequential epitopes. Nevertheless, in the past decade the number of reports of synthetic molecules capable of blocking protein−protein interactions in a specific manner has grown steadily.[1] On the other hand, few protein mimetics with effector functions, that can both bind to a cell surface receptor and activate downstream signaling pathways have been described.

Ligand-induced oligomerization or aggregation of cell surface receptors (e.g., cytokine receptors, receptor tyrosine kinases, tumor necrosis factor (TNF) receptors, T-cell receptors (TCRs), Toll-like receptors (TLRs), and G-protein coupled receptors (GPCRs) for naming a few) is an important mechanism to initiate and control signaling in a number of biological processes.[3−8] In this context, (small) synthetic molecules binding avidly to multiple copies of a receptor may be used to activate signaling pathways similar to the cognate ligand. Early studies

[†] Immunologie et Chimie Thérapeutiques (ICT).

[‡] Present Address: Institute of Biological Science and Technology, Beijing Jiaotong University, 3 Shang Yuan Cun, Haidian District, 100044 Beijing, China.

(1) For review, see: (a) Davis, J. M.; Tsou, L. K.; Hamilton, A. D. *Chem. Soc. Rev.* **2007**, *36*, 326−334. (b) Zhao, L.; Chmielewski, J. *Curr. Opin. Struct. Biol.* **2005**, *15*, 31−34. (c) Yin, H.; Hamilton, A. D. *Angew. Chem., Int. Ed.* **2005**, *44*, 4130−4163. (d) Arkin, M. R.; Wells, J. A. *Nat. Rev. Drug Discovery* **2004**, *3*, 301−317. (e) Pagliaro, P.; Felding, J.; Audouze, K.; Nielsen, S. J.; Terry, R. B.; Krog-Jensen, C.; Butcher, S. *Curr. Opin. Chem. Biol.* **2004**, *8*, 442−449. (f) Berg, T. *Angew. Chem., Int. Ed.* **2003**, *42*, 2462−2481; *Angew. Chem.* **2003**, *115*, 2566−2586. (g) Toogood, P. L. *J. Med. Chem.* **2002**, *45*, 1543−1558. (h) Peczuh, M. W.; Hamilton, A. D. *Chem. Rev.* **2000**, *100*, 2749−2494. (i) Cochran, A. G. *Chem. Biol.* **2000**, *7*, R85−R94.

(2) (a) Lo Conte, L.; Chothia, C.; Janin, J. *J. Mol. Biol.* **1999**, *285*, 2177−2198. (b) Chakrabarti, P.; Janin, J. *Proteins* **2002**, *47*, 334−343.

(3) (a) Austin, D. J.; Crabtree, G. R.; Schreiber, S. L. *Chem. Biol.* **1994**, *1*, 131−6. (b) Klemm, J. D.; Crabtree, G. R.; Schreiber, S. L. *Annu. Rev. Immunol.* **1998**, *16*, 569−592.

(4) (a) Heldin, K.-H. *Cell* **1995**, *80*, 214−223. (b) Heldin, C. H.; Ostman, A. *Growth Factor Rev.* **1996**, *7*, 3−10.

(5) (a) Schlessinger, J. *Cell* **2000**, *103*, 211−225. (b) Lemmon, M. A.; Schlessinger, J. *Methods Mol. Biol.* **1998**, *84*, 49−71.

(6) (a) Germain, R. N. *Curr. Biol.* **1997**, *7*, R640−644. (b) Alarcón, B.; Swamy, M.; van Santen, H. M.; Schamel, W. W. A. *EMBO J.* **2006**, *7*, 490−495.

(7) (a) Ozinsky, A.; Underhill, D. M.; Fontenot, J. D.; Hajjar, A. M.; Smith, K. D.; Wilson, C. B.; Schroeder, L.; Aderem, A. *Proc. Natl. Acad. Sci. U.S.A.* **2000**, *97*, 13766−13771. (b) Choe, J.; Kelker M. S.; Wilson, I. A. *Science* **2005**, *309*, 581−585. (c) Kirk, P.; Bazan, J. *Immunity*, **2005**, *23*, 347−350.

 10.1021/ja073169m CCC: $37.00

on synthetic multivalent systems (mainly for antagonizing unwanted biological processes) have clearly demonstrated that it is possible through polyvalency to achieve tight binding with ligands of low or modest surface areas.[9−13] The possibility to create molecules with effector functions through multivalency has been recognized more recently.[11−15] In the field of cytokine and growth factor mimetics, dimeric peptides, C_2-symmetric organic molecules as well as dendrimers capable of dimerizing and activating erythropoietin receptor (EPO-R), thrombopoietin receptor (TPO-R), granulocyte-colony stimulating factor (G-CSF) receptor, nerve growth factor (NGF) receptor TrkA, or neurotrophin-3 (NT-3) receptor TrkC are worth mentioning.[16,17]

While protein−ligand induced dimerization is the mechanism of activation of receptors for cytokines and growth factors, signaling by members of the tumor necrosis factor receptor (TNF-R) family involves receptor trimerization.[18,19] The geometry of the resulting ligand−receptor complex is favorable to the formation of an intracellular signaling complex.[4a,18] TNF-R family members can transduce a variety of intracellular signals culminating in cell proliferation, differentiation, survival, and death. Most of the 19 ligands and 29 receptors of the TNF/TNF-R superfamilies play an active role in the development, maintenance, and function of the immune system.[18] A few members are also implicated in other physiological processes such as bone remodeling or development of skin appendages. CD40 is expressed on antigen-presenting cells (APCs) such as dendritic cells (DCs) and B cells and, by interacting with its ligand CD40L (CD154), leads to their activation and differentiation.[20] Blockade of the CD40/CD40L pathway is a potential immunomodulatory strategy for B- and T-cell-mediated diseases. Administration of anti-CD40L antibodies has given encouraging results in the treatment of experimental autoimmune diseases as well as in the treatment of allograft rejection.[21,22] Alternatively, triggering CD40 signaling *in vivo* can be used to enhance immunity against intracellular pathogens or tumor cells. The use of agonistic anti-CD40 antibodies for example has been shown to increase the efficacy of peptide-based antitumor vaccines.[23] These findings support a clinical use of CD40-stimulating agents as components of anticancer immunotherapies or anti-infectious vaccines. Like other members of the TNF family, CD40L monomers self-assemble around a three-fold symmetry axis to form noncovalent homotrimers that can each bind three receptor molecules. The crystal structure of CD40L extracellular domain homotrimers[24] and a homology model of the CD40L/CD40 complex[25] have provided the basis for the

(8) (a) Bouvier, M. *Nat. Rev. Neurosci.* **2001**, 2, 274−286. (b) George, S. R.; O'Dowd, B. F.; Lee, S. P. *Nat. Rev. Drug Discovery* **2002**, *1*, 808−820. (c) Park, P. S.; Filipek, S.; Wells, J. W.; Palczewski, K. *Biochemistry* **2004**, *43*, 15643−15656. (d) Prinster, S. C.; Hague, C.; Hall, R. A. *Pharmacol. Rev.* **2005**, *57*, 289−298. (e) Bulenger, S.; Marullo, S.; Bouvier, M. *Trends Pharmacol. Sci.* **2005**, *26*, 131−137.

(9) For early examples of carbohydrate-based multivalent inhibitors (glycopolymers and glycodendrimers) of influenza virus hemagglutinin binding to host cells, see: (a) Spaltenstein, A.; Whitesides, G. M. *J. Am. Chem. Soc.* **1991**, *113*, 686−687. (b) Sabesan, S.; Duus, J. O.; Domaille, P.; Kelm, S.; Paulson, J. C. *J. Am. Chem. Soc.* **1991**, *113*, 5865−5866. (c) Gamian, A.; Chomik, M.; Laferriere, C. A.; Roy, R. *Can. J. Microbiol.* **1991**, *37*, 233−237. (d) Kingery-Wood, J. E.; Williams, K. W.; Sigal, G. B.; Whitesides, G. M. *J. Am. Chem. Soc.* **1992**, *114*, 7303−7305. (e) Sparks, M. A.; Williams, K. W.; Whitesides, G. M. *J. Med. Chem.* **1993**, *36*, 778−783. (f) Roy, R.; Pon, R. A.; Tropper, F. D.; Andersson, F. O. *J. Chem. Soc., Chem. Commun.* **1993**, 264−265. (g) Roy, R.; Zanini, D.; Meunier, S. J.; Romanowska, A. *J. Chem. Soc., Chem. Commun.* **1993**, 1869−1872.

(10) Selected recent examples of multivalent inhibitors: (a) Dimick, S. M.; Powell, S. C.; McMahon, S. A.; Moothoo, D. N.; Naismith, J. H.; Toone, E. J. *J. Am. Chem. Soc.* **1999**, *121*, 10286−10296. (b) Kitov, P. I.; Sadowska, J. M.; Mulvey, G.; Armstrong, G. D.; Ling, H.; Pannu, N. S.; Read, R. J.; Bundle, D. R. *Nature* **2000**, *403*, 669−672. (c) Merritt, E. A.; Zhang, Z.; Pickens, J. C.; Ahn, M.; Hol, W. G.; Fan, E. *J. Am. Chem. Soc.* **2002**, *124*, 8818−8824. (d) Gestwicki, J. E.; Cairo, C. W.; Strong, L. E.; Oetjen, K. A.; Kiessling, L. L. *J. Am. Chem. Soc.* **2002**, *124*, 14922−14933; Gradl, S. N.; Felix, J. P.; Isacoff, E. Y.; Garcia, M. L.; Trauner, D. *J. Am. Chem. Soc.* **2003**, *125*, 12668−12669. (e) Thumshirn, G.; Hersel, U.; Goodman, S. L.; Kessler, H. *Chem. Eur. J.* **2003**, *9*, 2717−2725. (f) Boturyn, D.; Coll, J.-L.; Garanger, E.; Favrot, M.-C.; Dumy, P. *J. Am. Chem. Soc.* **2004**, *126*, 5730−5739. (g) Wolfenden, M. L.; Cloninger, M. J. *J. Am. Chem. Soc.* **2005**, *127*, 12168−12169. (h) Arosio, D.; Fontanella, M.; Baldini, L.; Mauri, L.; Bernardi, A.; Casnati, A.; Sansone, F.; Ungaro, R. *J. Am. Chem. Soc.* **2005**, *127*, 3660−3661.

(11) For early examples of bivalent opioid ligands, see: (a) Portoghese, P. S. *J. Med. Chem.* **2001**; *44*, 2259−2269. (b) Erez; M.; Takemori, A. E.; Portoghese, P. S. *J. Med. Chem.* **1982**, *25*, 847−849; Portoghese, P. S.; Larson, D. L.; Sayre, L. M.; Yim, C. B. (c) Ronsisvalle, G.; Tam, S. W.; Takemori, A. E. *J. Med. Chem.* **1986**, *29*, 1855−1861.

(12) Choi, S. K. *Synthetic Multivalent Molecules: Concepts and Biochemical Applications*; Wiley-Interscience: Hoboken, NJ, 2004.

(13) For reviews, see: (a) Mammen, M.; Choi, S.-K.; Whitesides, G. M. *Angew. Chem., Int. Ed.* **1998**, *37*, 2755−2794. (b) Kiessling, L. L.; Gestwicki, J. E.; Strong, L. E. *Curr. Opin. Chem. Biol.* **2000**, *4*, 696−703. (c) Kiessling, L. L.; Pohl, N. L. *Chem. Biol.* **1996**, *3*, 71−77.

(14) For review, see: Kiessling, L. L.; Gestwicki, J. E.; Strong, L. E.; *Angew. Chem., Int. Ed.* **2006**, 45, 2348−2368.

(15) Selected examples: (a) Gestwicki, J. E.; Strong, L. E.; Kiessling, L. L. *Chem. Biol.* **2000**, *7*, 583−591. (b) Gestwicki, J. E.; Kiessling, L. L. *Nature* **2002**, *415*, 81−84. (c) Kramer, R. H.; Karpen, J. W. *Nature* **1998**, *395*, 710−713. (d) Pattarawarapan, M.; Reyes, S.; Xia, Z.; Zaccaro, M. C.; Saragovi, H. U.; Burgess, K. *J. Med. Chem.* **2003**, *46*, 3565−3567. (e) Puffer, E. B.; Pontrello, J. K.; Hollenbeck, J. J.; Kink, J. A.; Kiessling, L. L. *ACS Chem. Biol.* **2007**, *2*, 252−262.

(16) Reviews on small molecule cytokine mimetics: (a) Whitty, A.; Borysenko, C. W. *Chem. Biol.* **1999**, *6*, R107−R118.

(17) (a) Wrighton, N. C.; Farrell, F. X.; Chang, R.; Kashyap, A. K.; Barbone, F. P.; Mulcahy, L. S.; Johnson, D. L.; Barrett, R. W.; Jolliffe, L. K.; Dower, W. J. *Science* **1996**, *273*, 458−463. (b) Livnah, O.; Stura, E. A.; Johnson, D. L.; Middleton, S. A.; Mulcahy, L. S.; Wrighton, N. C.; Dower, W. J.; Jolliffe, L. S. Wilson, I. A. *Science* **1996**, *273*, 464−471. (c) Johnson, D. L.; Farrell, F. X.; Barbone, F. P.; McMahon, F. J.; Tullai, J.; Kroon, D.; Freedy, J.; Zivin, R. A.; Mulcahy, L. S.; Jolliffe, L. K. *Chem. Biol.* **1997**, *4*, 939−950. (d) Cwirla, S. E.; Balasubramanian, P.; Duffin, D. J.; Wagstrom, C. R.; Gates, C. M.; Singer, S. C.; Davis, A. M.; Tansik, R. L.; Mattheakis, L. C.; Boytos, C. M.; Schatz, P. J.; Baccanari, D. P.; Wrighton, N. C.; Barrett, R. W.; Dower, W. J. *Science* **1997**, *276*, 1696−1699. (e) Qureshi, S. A.; Kim, A. M.; Konteatis, Z.; Biazzo, D. E.; Motamedi, H.; Rodrigues, R.; Boice, J. A.; Calaycay, J. R.; Bednarek, M. A.; Griffin, P.; Gao, Y.-D.; Chapman, K.; Mark, D. F. *Proc. Natl. Acad. Sci. U.S.A.* **1999**, *12*, 12156−12161. (f) Goldberg, J.; Jin, Q.; Ambroise, Y.; Satoh, S.; Desharnais, J.; Capps, K.; Boger, D. L. *J. Am. Chem. Soc.* **2002**, *124*, 544−555. (g) Tian, S.-S.; Lamb, P.; King, A. G.; Miller, S. G.; Kessler, L.; Luengo, J. I.; Averill, L.; Johnson, R. K.; Gleason, J. G.; Pelus, L. M.; Dillon, S. B.; Rosen, J. *Science* **1998**, *281*, 257−259. (h) Pattarawarapan, M.; Reyes, S.; Xia, Z.; Zaccaro, M. C.; Saragovi, H. U.; Burgess, K. *J. Med. Chem.* **2003**, *46*, 3565−3567.

(18) (a) Bodmer, J. L.; Schneider, P.; Tschopp, J. *Trends Biochem. Sci.* **2002**, *27*, 19−26. (b) Locksley, R. M.; Killen, N.; Lenardo, M. J. *Cell* **2001**, *104*, 487−501.

(19) Although the conventional view is that members with the TNF-R family exist as independently diffusing monomeric species and trimerize upon ligand binding, some evidence suggests however, that several of these receptors may exist as pre-assembled oligomers prior to ligand binding. It has been shown that a conserved domain in the extracellular region of TNF-R, Trail receptor 1, and CD40, distal from the domain that interacts with the ligand, serves as a preligand-binding assembly domain (PLAD). Chan, F. K.; Chun, H. J.; Zheng, L.; Siegel, R. M.; Bui, K. L.; Lenardo, M. J. *Science* **2000**, *288*, 2351−2354.

(20) For reviews, see: (a) van Kooten, C.; Banchereau, J. *J. Leuk. Biol.* **2000**, *67*, 1−17. (b) Diehl, L.; Den, Boer, A. T.; van der Voort, E. I.; Melief, C. J.; Offringa, R.; Toes, R. E. *J. Mol. Med.* **2000**, *78*, 363−371. (c) Grewal, I. S.; Flavell, R. A. *Annu. Rev. Immunol.* **1998**, *16*, 111−135. (d) Van Kooten, C.; Banchereau, J. *Adv. Immunol.* **1996**, *61*, 1−77. (e) Grewal, I. S.; Flavell, R.A. *Immunol. Today* **1996**, *17*, 410−414. (f) Noelle, R. J. *Immunity* **1996**, *4*, 415−419.

(21) (a) Howard, L. M.; Miga, A. J.; Vanderlugt, C. L.; Dal Canto, M. C.; Laman, J. D.; Noelle, R. J.; Miller, S. D. *J. Clin. Invest.* **1999**, *103*, 281−290. (b) Kirk, A. D.; et al. *Nat. Med.* **1999**, *5*, 686−693.

(22) Phase I/II studies in humans with lupus nephritis or multiple sclerosis revealed significant immunomodulatory effects of anti-CD40L monoclonal antibody treatment. However, because of some thromboembolic complications in early clinical trials, further human studies with anti-CD40L antibody have been temporary halted, and future clinical use is uncertain. See comment in: Couzin, J. *Science* **2005**, *307*, 1712−1715.

(23) (a) Diehl, L.; den Boer, A. T.; Schoenberger, S. P.; van der Voort, E. I.; Schumacher, T. N.; Melief, C. J.; Offringa, R.; Toes, R. E. *Nat. Med.* **1999**, *5*, 774−779. (b) van Mierlo, G. J.; den Boer, A. T.; Medema, J. P.; van der Voort, E. I.; Fransen, M. F.; Offringa, R.; Melief, C. J.; Toes, R. E. *Proc. Natl. Acad. Sci. U.S.A.* **2002**, *99*, 5561−5566.

(24) Karpusas, M.; Lucci, J.; Ferrant, J.; Benjamin, C.; Taylor, F. R.; Strauch, K.; Garber, E.; Hsu, Y. M. *Structure* **2001**, *9*, 421−429.

(25) Singh, J.; Garber, E.; Van Vlijmen, H.; Karpusas, M.; Hsu, Y. M.; Zheng, Z.; Naismith, J.; Thomas, D. *Protein Sci.* **1998**, *7*, 1124−1135.

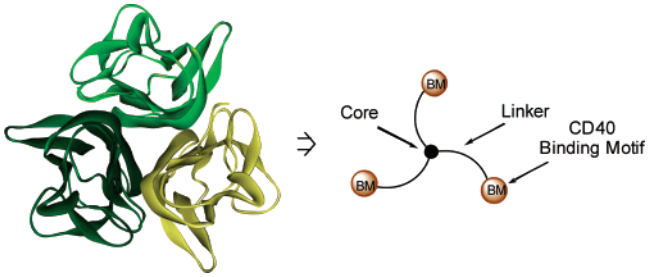

Figure 1. X-ray structure of CD40L homotrimer (PDB 1ALY)[22] viewed down the C_3 axis and schematic representation of trimeric architecture used as CD40L mimetics.

rational design and synthesis of a first-generation of CD40L mimetics.[26,27] We have shown that rigid trimeric scaffolds can serve to distribute a CD40-binding motif with geometry and distances that could match that of the natural CD40L protein (Figure 1). A short loop sequence from the surface of CD40L encompassing three "hot-spot" residues (Lys[143], Tyr[145], and Tyr[146] in the AA″ loop) critical for binding to CD40, was initially chosen as a CD40-binding motif.

The gain in avidity that could result from a multivalent interaction with CD40 molecules was expected to overcome the relatively low binding energy of the short tetrapeptide sequence. Two trimeric molecules **A-1** and **B-1** built on the rigid *cyclo*-(Lys-D-Ala)$_3$ and *cyclo*-(β^3-HLys) peptide rings **A** and **B**, respectively (see Chart 1), with amino hexanoic acid (Ahx) residues as additional spacer arms were found to bind in a specific manner to CD40 and to compete with the binding of CD40L homotrimers.[26,27] In various cell-based assays, **A-1** and **B-1** displayed some effector functions of the much larger recombinant CD40L homotrimers, i.e., induction of apoptosis of B lymphomas and maturation of DCs. Both CD40L mimetics were shown recently to be effective *in vivo* and to promote the control of *Trypanosoma cruzi* (i.e., the etiological agent of the *Chagas'*disease) infection in an experimental mouse model by overcoming the immunosuppression usually induced by the parasite.[28] However, the molecular determinants of the design of CD40L mimetics (hereby referred to as "*miniCD40Ls*") with optimal CD40 binding properties and effector functions are not yet fully delineated. To assess the contribution of each individual component of the trivalent architecture, we have now undertaken a detailed study by systematically varying the shape and the valency of the core structure, the geometry and the length of the spacer arm as well as the nature of the CD40 binding motif.

Results and Discussion

Ligand Synthesis. All CD40L mimetics described in this study (except **E-1**, see Supporting Information) were synthesized according to Scheme 1 by fragment coupling in solution of a fully protected peptide fragment encompassing the receptor binding motif and a spacer arm, to the corresponding amino-functionalized core structure **A-0** to **L-0** (R = H). The protected CD40-binding peptides with their linkers were prepared on solid support starting from a 2-chlorotrityl chloride resin as illustrated in Scheme 2 for the Lys-Gly-Tyr-Tyr-Ahx sequence. Peptide assembly on core structures was generally performed with BOP[29] as the coupling agent in DMF for 24 h, after which the crude fully protected multimeric construct recovered by filtration after precipitation with a saturated $NaHCO_3$ solution was washed extensively with ethyl acetate and dried under high vacuum. All protecting groups were removed by treatment with trifluoroacetic acid (TFA) to afford crude ligands. Finally, ligands were purified by C_{18} RP-HPLC and recovered in overall yields ranging from 6 to 37%. It is noteworthy that the synthesis of **A-1** was routinely achieved on >100 mg scale with an overall yield exceeding 25%. In an optimized process, the linear peptide precursor of scaffold **A**, H-(Lys(Boc)-D-Ala)$_3$-OH was assembled by solid-phase synthesis on a 2-chlorotrityl chloride resin. All ligands were identified by matrix-assisted laser desorption/ionization mass spectrometry (MALDI-MS) and their homogeneity was assessed by C_{18} RP-HPLC with purity of all peptides determined to be >99%, (see Supporting Information for detailed experimental procedures and characterization of all investigated ligands).

Variations in Shape and Size of the Central Core. The nature of a scaffold for polyvalent display can significantly impact on the biological activity of synthetic multivalent ligands. Features such as geometry, valency, and rigidity must be carefully tailored to ensure effective distribution of appended recognition patterns. This has been recognized in a number of multivalent systems with a variety of poly(oligo-)valent scaffolds (e.g., small synthetic scaffolds, dendrimers, polymers, liposomes, proteins, and viral particles).[9,10,12−14] Our previous finding that CD40L mimetics based on trimeric architectures **A** and **B** but not branched **E** exhibit effector functions in several cellular assays (maturation of D1 dendritic cell line,[30] apopotosis of B lymphoma cells[31]) and promote control of parasitemia during experimental *T. cruzi* infections in mice tend to suggest that the rigidity of the central core is one determinant of the activity of CD40L mimetics.[26a,27] This can be rationalized in terms of the minimization of the conformational entropic cost.[13a] It also suggests that effective trivalent display of a given CD40-binding motif with geometry and distances that match those in the cognate protein trimer imposes constraints on the overall geometry and dimensions of the core + linker element. To ascertain this trend, we have now considered an enlarged set of trimeric architectures falling into three categories (Chart 1): macrocyclic (**A**−**D**), branched (**E**,**F**), and heterocyclic (**G**−**I**), varying in size (**A** ≈ **C** > **B** > **I** > **G** > **E** > **H** > **F**, based on fully extended structures) and rigidity. Partially *N*-methylated *cyclo*-D,L-α-peptide **C** which displays a smaller number of H-bond donors than **A** was intended to modulate the possible self-assembling properties of the resulting ligands.[32] A macrocyclic ligand with receptor-binding motifs attached to the upper rim of a calix[6]triamine core structure (type **D**)[33] was designed

(26) (a) Fournel, S.; Wieckowski, S.; Sun, W.; Trouche, N.; Dumortier, H.; Bianco, A.; Chaloin, O.; Habib, M.; Peter, J.-C.; Schneider, P.; Vray, B.; Toes, R. E.; Offringa, R.; Melief, C. J. M.; Hoebeke, J.; Guichard, G. *Nat. Chem. Biol.* **2005**, *1*, 377−382. (b) Bianco, A.; Fournel, S.; Wieckowski, S.; Hoebeke, J.; Guichard, G. *Org. Biomol. Chem.* **2006**, *4*, 1461−1463.
(27) (a) Hymowitz, S. G.; Ashkenazi, A. *Nat. Chem. Biol.* **2005**, *1*, 353−354. (b) Gibson, S. E.; Castaldi, M. P. *Angew. Chem., Int. Ed.* **2006**, *45*, 4718−4720.
(28) Habib, M.; Chamekh, M.; Noval, Rivas, M.; Wieckowski, S;, Sun, W.; Bianco, A.; Trouche, N.; Chaloin, O.; Dumortier, H.; Goldman, M.; Guichard, G.; Fournel, S.; Vray, B. *J. Immunol.* **2007**, *178*, 6700−6704.
(29) Castro, B.; Dormoy, J. R.; Evin, G.; Selve, C. *Tetrahedron Lett.* **1975**, 1219−1222.
(30) Schuurhuis, D. H.; Laban, S.; Toes, R. E. M.; Ricciardi-Castagnoli, P.; Kleijmeer, M. J.; van der Voort, E. I. H.; Rea, D.; Offringa, O.; Geuze, H. J.; Melief, C. J. M.; Ossendorp, F. *J. Exp. Med.* **2000**, *192*, 145−150.
(31) B lymphoma cells undergo apoptosis upon engagement of CD40 by recombinant CD40L. See: Frisan, T.; Donati, D.; Cervenak, L.; Wilson, J.; Masucci, M. G.; Bejarano, M. T. *Int. J. Cancer* **1999**, *83*, 772−779.
(32) Bong, D. T.; Clark, T. D.; Granja, J. R.; Ghadiri, M. R. *Angew. Chem., Int. Ed.* **2001**, *40*, 988−1011 and refs therein.

Chart 1. Trimeric Architectures and Ligands Based on Scaffolds **A-I**

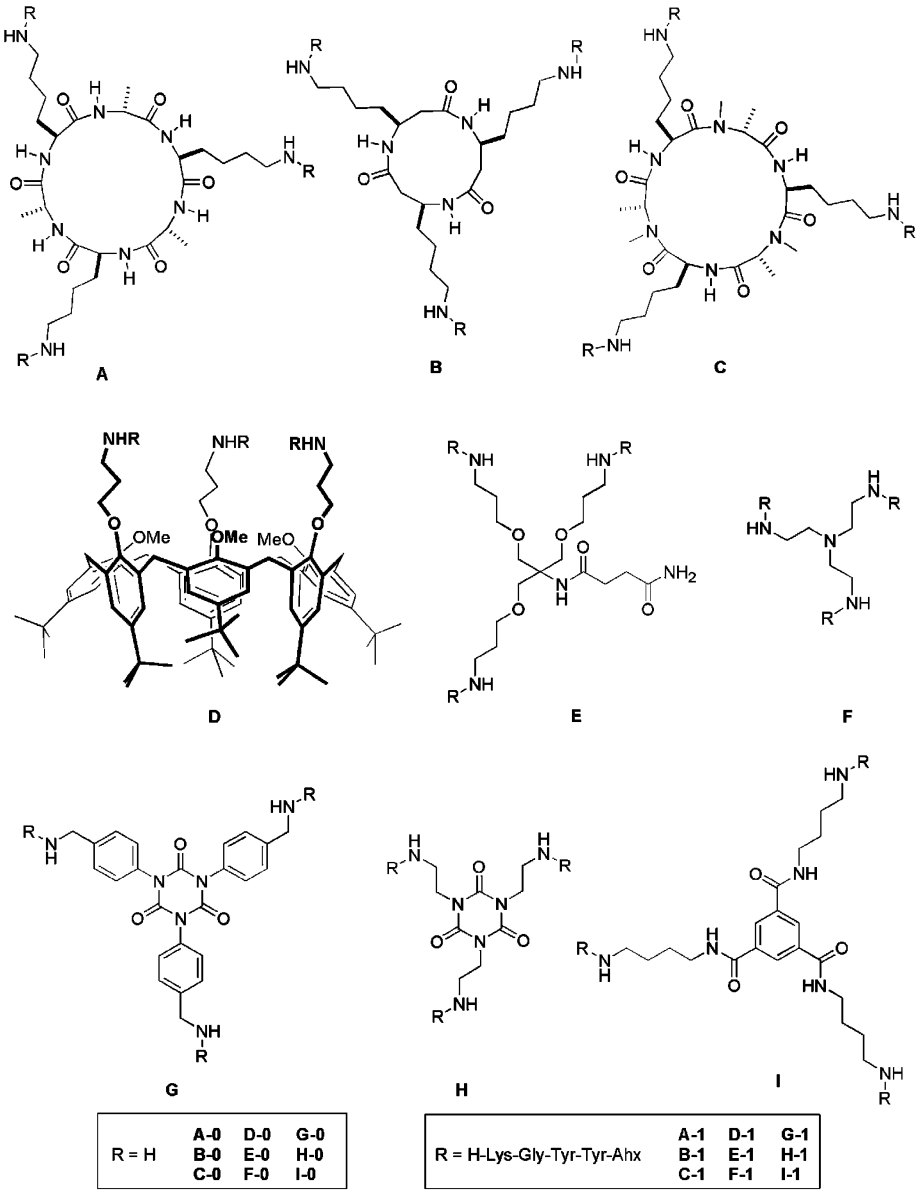

Scheme 1. General Synthetic Approach to Trimeric CD40L Mimetics

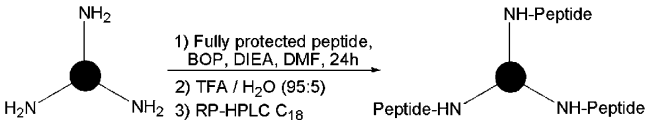

to investigate the effect of a more axial (assuming a cone conformation) distribution of the CD40-binding motif.[34]

The corresponding ligands **A-1** to **I-1** obtained by appending the pentapeptide sequence Lys-Gly-Tyr-Tyr-Ahx (**1**) have been evaluated for binding to rshCD40:mIg [a bivalent form of CD40 consisting of recombinant human CD40 fused to a mouse IgG Fc domain (see Figure S1 in Supporting Information)] using surface plasmon resonance (SPR) and for their capacity to induce apoptosis of the human B lymphoma cell line BL41 (Figures 2 and 3).

Screening of molecules **A-1** to **I-1** at 250 nM in a SPR binding assay with immobilized rshCD40:mIg confirmed macrocyclic **A-1** and **B-1** and newly identified heterocyclic **G-1** as the best CD40 binders in the series in terms of binding capacity and interaction stability (Figures 2a, S2, and S3). A similar trend was observed when analyzing kinetic binding parameters calculated from SPR sensorgrams acquired for various concentrations of *miniCD40Ls* (k_a versus k_d plots with isoaffinity lines are shown in Figure 2b). Kinetic values were all derived from the 1:1 interaction Langmuir model (see Experimental Section for description of equations used and Figure S3 for raw SPR data).[35,36] Whereas the majority of CD40L/CD40 interactions showed binding kinetics suitable for determination of the kinetic

(33) Gac, S.; Zeng, X.; Reinaud, O.; Jabin, I. *J. Org. Chem.* **2005**, *70*, 1204−1210.

(34) For use of calixarenes as multivalent templates and for the recognition of protein surfaces, see: (a) Baldini, L.; Casnati, A.; Sansone, F.; Ungaro, R. *Chem. Soc. Rev.* **2007**, 36, 254−266. (b) Reference 9g. (c) Park, H. S.; Lin Q.; Hamilton, A. D. *Proc. Natl. Acad. Sci. U.S.A.* **2002**, *99*, 5105−5109. (d) Blaskovich, M. A.; Lin, Q.; Delarue, F. L.; Sun, J.; Park, H. S.; Coppola, D.; Hamilton, A. D.; Sebti, S. M. *Nat. Biotechnol.* **2000**, *18*, 1065−1070. (e) Park, H. S.; Lin, Q.; Hamilton, A. D. *J. Am. Chem. Soc.* **1999**; *121*, 8−13.

Scheme 2. Synthesis of the Protected Pentapeptide Boc-Lys(Boc)-Gly-Tyr(O*t*Bu)-Tyr(O*t*Bu)-Ahx-OH (**1**) (See Supporting Information for Details)[a]

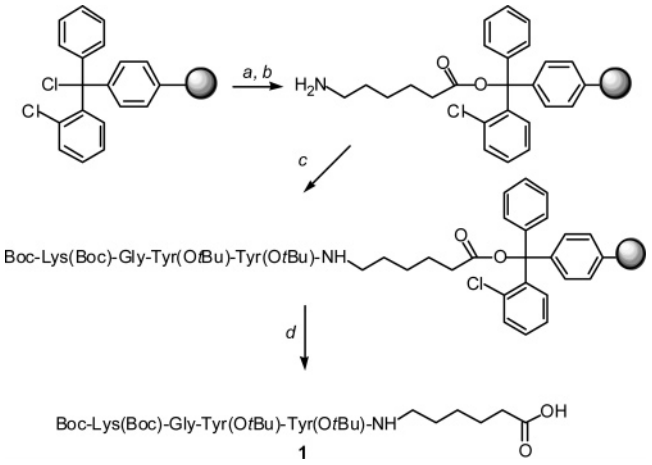

[a]Conditions: (a) Fmoc-6-aminocaproic acid, DIEA, CH_2Cl_2; (b) 25% piperidine/DMF; (c) SPPS: Fmoc-Xaa-OH, BOP, HOBt, DIEA, DMF; (d) HFIP/CH_2Cl_2 (60:40 v/v).

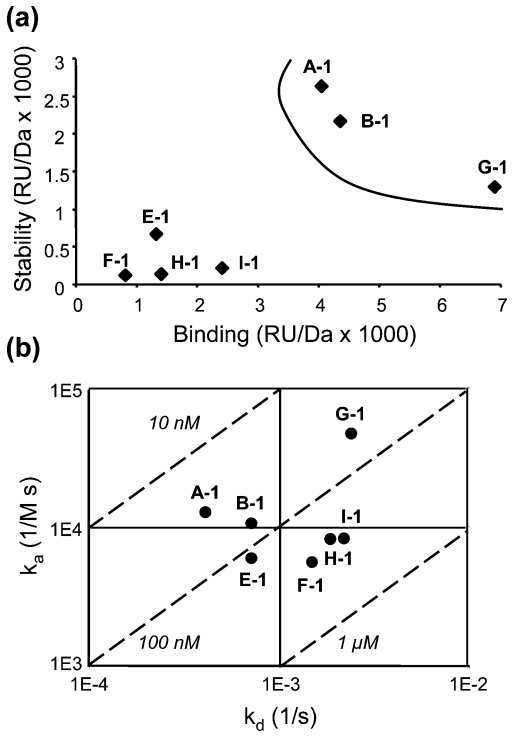

Figure 2. Comparison of compounds **A-1** to **I-1** for binding to CD40 by surface plasmon resonance (SPR). (a) Screening of the molecules in a comparative assay at 250 nM. Binding and stability report points for each *miniCD40L* were determined from the association and dissociation phases on the sensorgrams at 235 and 250 s, respectively (see Figures S2 and S3). Responses were baseline substracted and adjusted for the refractive index (RI) and the molecular weight of each molecule. Molecules are thus compared in a plot reflecting the extent of binding and stability of the interaction with CD40. The best ligands are encircled. (b) Graphical summary of the data generated from different concentrations of the mimetics. Kinetics values were all derived from the 1:1 Langmuir model. All results are representative of at least two independent experiments.

rate constants, SPR analysis was hampered for ligands **C-1** and **D-1** (partially *N*-methylated cyclo-D,L-hexapeptide and calix-[6]arene cores, respectively) because of the formation of aggregates in the conditions of the assay. Trimeric ligands were also compared in an inhibition SPR assay as shown in Figure

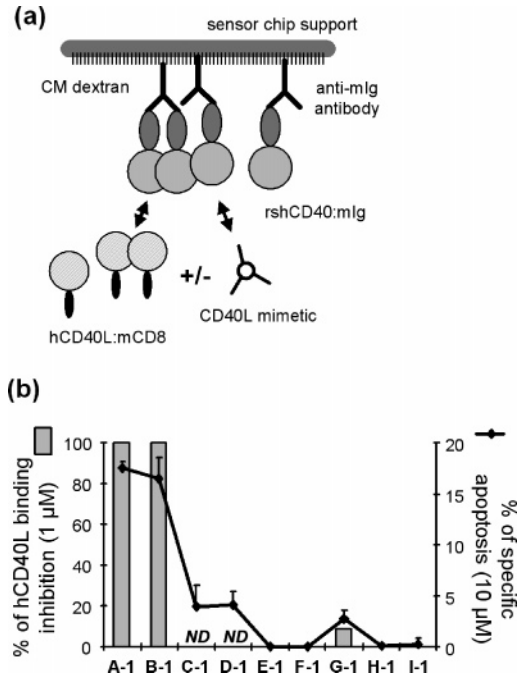

Figure 3. Comparison of compounds **A-1** to **I-1** for their ability to inhibit binding of soluble human CD40L (hCD40L:mCD8) to CD40 and to induce apoptosis of the human B lymphoma cell BL41. (a) Schematic representation of the SPR inhibition experiment. (b) Gray bars: values of the inhibition experiments. Percentages of inhibition at 1 μM of mimetics are represented. They were derived from the slope of the CD40Ls mixed to the mimetics response signal substracted from the response signal of the mimetics alone. Results are representative of two independent experiments. ***ND***: not determinable because of aggregation; black line: induction of apoptosis of human lymphoma cell line BL41 after 16 h of treatment. Values compared are from percentages of specific apoptosis (see Experimental Section) obtained at 10 μM of the different mimetics. Results are expressed as means $\pm$ SEM of three independent experiments.

3a. At 1 μM, only **A-1** and **B-1** were found to significantly inhibit the binding of soluble recombinant hCD40L:mCD8 to rshCD40:mIg fusion protein (Figure 3b). Molecule **G-1** was only a weak inhibitor. In parallel, all ligands were screened in a cell-based assay (Figure 3b). Their capacity to induce apoptosis of CD40-positive human Burkitt B lymphoma cells was measured by the decrease of the mitochondrial membrane potential ($\Delta\psi_m$) using $DiOC_6(3)$ dye as previously described.[26a,37] **A-1** and **B-1** induced a high level of apoptosis at 10 μM, whereas all remaining ligands were only weakly active (**C-1**, **D-1**, **G-1**) or ineffective (**E-1**, **F-1**, **H-1**, **I-1**).

Ligands **A-1** and **B-1** differ from other tested ligands by the shape of their central core. The general structural features of

(35) In the case of **A-1**, SPR data fit better with a trivalent model than with the classical "Langmuir 1:1" monovalent one [Chi square (χ^2) values which indicate that the accuracy of the fits are 0.43 and 0.85, respectively], suggesting that this interaction is of one *miniCD40L* for three CD40 receptors stoichiometry. Wieckowski, S.; Trouche, N.; Chaloin, O.; Guichard, G.; Fournel, S.; Hoebeke, J. *Biochemistry*, **2007**, *46*, 3482−3493.

(36) Because of substantial but unknown contribution of avidity effects to the strength of binding that results from CD40 being immobilized to high density on the CM5 sensor chip, the affinities measured in our SPR binding assay represent apparent binding affinities rather than true K_D values. For an interesting discussion on the determination of true K_D values for TNF family ligands binding to their cognate receptors and introduction of a "solution-phase Biacore binding assay", see : Day, E. S.; Cachero, T. G.; Qian, F.; Sun, Y.; Wen, D.; Pelletier, M.; Hsu, Y. M.; Whitty, A. *Biochemistry* **2005**, *44*, 1919−1931.

(37) Quantification of **A-1**-mediated apoptosis in Burkitt lymphoma cells by an annexin V−propidium iodide colabeling technique (which enables the recognition of early and late apoptotic cells) and by terminal deoxynucleotide transferase dUTP nick-end labeling (TUNEL) gave comparable results (ref 26a and data not shown).

Chart 2

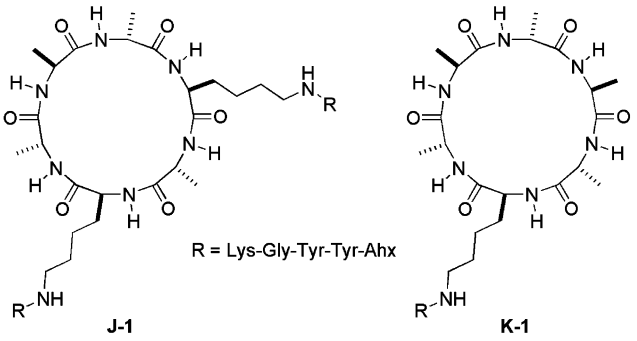

cyclo-(Xaa-D-Xbb)$_n$ and *cyclo*-(β^3-HXaa)$_n$ peptides have been extensively investigated both in solution by NMR spectroscopy and in the solid state by XRD and PXRD.[32,38−41] In both series, the peptide backbone generally adopts a flat-ring conformation with side chains occupying equatorial positions along the ring's edge.[42] The results obtained by SPR and in cell-based assays with compounds **A-1** to **I-1** suggest in first approximation that a radial distribution of the CD40-binding motif is preferred. Among all ligands tested, **A-1** and **B-1** are those potentially providing the longest distance between the center of the trivalent system and the NH connecting the Ahx linker. Thus, our data also support the view that the distance between the center of the trivalent system and the NH of the flexible linker connecting the CD40 binding motif should be above a minimum length (vide infra, section on modulation of the linker length).

Comparison to Mono-, Di-, and Tetravalent Systems. In the next series of experiments, the importance of a C_3-symmetric trivalent display was assessed by systematically varying the number of CD40 recognition elements appended to the cyclic D,L-peptide core (Chart 2).

We found that removing one CD40-binding motif while maintaining a radial distribution (**A-1** → **J-1**) resulted in a strong decrease of the CD40-binding capacity (Figure 4) and biological effects, i.e., apoptosis of human B lymphoma cells (Figure 5a) and maturation of mouse dendritic cells D1 (Figure 5b).[30] Not surprisingly, ligand **K-1** with only one CD40-binding motif appended to a cyclic D,L-hexapeptide core as well as the corresponding H-Lys-Gly-Tyr-Tyr-Ahx-OH pentapeptide[26a] was inactive.

We also investigated higher-order multimeric structures. A C_4-symmetric tetrameric analogue of **A-1** based on *cyclo*-(Lys-D-Ala)$_4$,[40] **L-1**, was synthesized and tested for CD40 binding and B lymphoma apoptosis (Figure 6). However, **L-1** turned out to be less soluble than **A-1**. Although SPR binding data obtained at low concentration between 6 nM and 100 nM may be indicative of specific binding, the C_4-symmetric ligand **L-1** was found to extensively aggregate above 200 nM under SPR conditions (see Supporting Information, Figure S4). Moreover, **L-1** was not able to induce significant apoptosis of B lymphomas at 10 μM. Overall these results together with those obtained with **J-1** and **K-1** support the view that C_3-symmetry of the core structure and radial distribution of appended peptides are both determinants of the activity of CD40L mimetics.

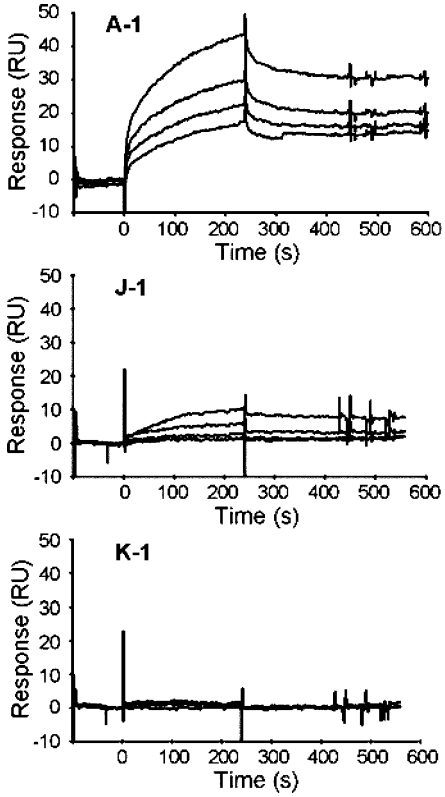

Figure 4. Influence of the valency of the ligands on their capacity to bind CD40. Direct binding of **A-1**, **J-1**, and **K-1** to CD40 as shown by SPR. All data were obtained for mimetics concentration from 100 to 800 nM.

Modulation of the Linker Portion. As discussed previously, the choice of an appropriate linker to connect the binding moieties in a multivalent system can be a determinant. Rather than a rigid linker difficult to optimize, we opted for rather flexible oligomethylene or oligo(ethylene glycol) type spacers that we felt to be more appropriate to sample conformational space. In the crystal structure of the CD40L homotrimer, the distance between the α carbon ($^{\alpha}$C) of each hot-spot residue, Lys^{143} to Tyr^{146}, and the centroid of the equilateral triangle formed by the $^{\alpha}$C of the three cognate residues in the trimer is between 17 and 22 Å. The α-amino group of the next residue in the sequence (Thr^{147}) is positioned ca. 16 Å apart from the center of the trimer. When designing ligands based on scaffold **A**, the Ahx linker was originally selected to approach this distance. If one assumes that the Lys(Ahx) side chain on the D,L-cyclohexapeptide core **A** adopts a fully extended conformation (∼14.9 Å) as in the crystal structure of a related Ahx-Ahx peptide segment[43] and that the diameter of the core cyclopeptide is ∼7.5−8 Å [based on the crystal structures[38,39] of related *cyclo*-

(38) For studies on partially *N*-alkylated C_3-symmetric cyclic D,L-hexapeptide structures, see: (a) Tomasi, L.; Lorenzi, G. P. *Helv. Chim. Acta* **1987**, *70*, 1012−1016. (b) Saviano, M.; Lombardi, A.; Pedone, C.; Di, Blasio, B.; Sun, X. C.; Lorenzi, G. P. *J. Incl. Phenom.* **1994**, *18*, 27−36. (c) Sun, X. C.; Lorenzi, G. P. *Helv. Chim. Acta* **1994**, *77*, 1520−1526.

(39) For crystal structures of *cyclo*-(L-Val-D-Val)$_3$ and *cyclo*-(L-Phe-D-Phe)$_3$ hexapeptides, see: Pavone, V.; Benedetti, E.; Di Blasio, B.; Lombardi, A.; Pedone, C.; Tomasich, L.; Lorenzi, G. *Biopolymers* **1989**, *28*, 215−223.

(40) For studies on cyclic D,L-octapeptides, see: (a) Ghadiri, M. R.; Granja, J. R.; Milligan, R. A.; McRee, D. E.; Khazanovich, N. *Nature* **1993**, *366*, 324−327. (b) Khazanovich, N.; Granja, J. R.; McRee, D. E.; Milligan, R. A.; Ghadiri, M. R. *J. Am. Chem. Soc.* **1994**, *116*, 6011−6012. (c) Hartgerink, J. D.; Granja, J. R.; Milligan, R. A.; Ghadiri, M. R. *J. Am. Chem. Soc.* **1996**, *118*, 43−50.

(41) (a) For the NMR structure determination of *cyclo*-(β^3-HGlu)$_3$ in D_2O, see: Gademann, K.; Seebach, D. *Helv. Chim. Acta* **1999**, *82*, 957−962. (b) For XRD studies of three stereoisomers of *cyclo*-(β^3-HAla)$_4$, see: Seebach, D.; Matthews, J. L.; Meden, A.; Wessels, T.; Baerlocher, C.; McCusker, L. B. *Helv. Chim. Acta* **1997**, *80*, 173−182.

(42) Although *cyclo*-L,D-peptides show propensity to self-assemble into H-bonded tubular stacks in the solid state and in nonpolar solvents, there is no indication that **A-1** aggregates in aqueous solution.

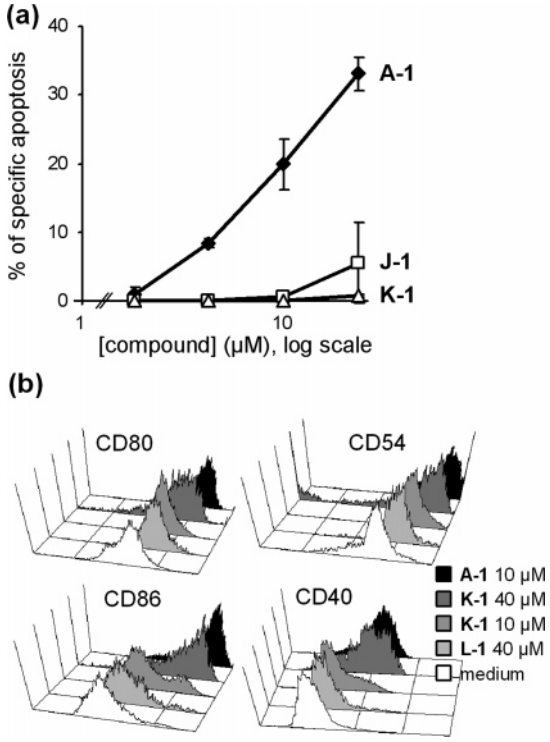

Figure 5. Influence of the valency on effector functions. (a) Induction of apoptosis of human lymphoma cell line BL41. Percentage of specific apoptosis measured by reduction of $DiOC_6(3)$ dye uptake (see Experimental Section) induced by the different mimetics at the indicated concentrations after 16 h of incubation. Results are expressed as means ± SD of two independent experiments. (b) Expression of the maturation markers (CD80, CD54, CD86, and CD40) by the mouse dendritic cell line D1 as measured by flow cytometry after 24 h of incubation with the different mimetics at the indicated concentrations; white histogram: medium control.

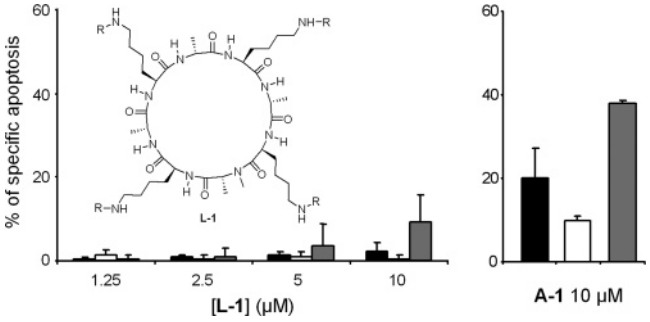

Figure 6. Tetrameric versus trimeric ligands. Percentage of specific apoptosis induced by **L-1** and **A-1** at the indicated concentrations after 16 h of incubation detected by reduction of $DiOC_6(3)$ dye uptake (see Experimental Section). Cells used in the assay are human lymphoma cells BL41 (black) which express CD40, Jurkat cells (white) which do not express CD40, and B lymphoma Raji cells (gray bars) which express high level of CD40. Results are expressed as means ± SEM of three independent experiments. Molecular structure of the tetravalent mimetic is shown in the inset.

(L-Val-D-Val)$_3$, *cyclo*-(L-Phe-D-Phe)$_3$, and *cyclo*-(*N*-MeLeu-D-Leu)$_3$], one can approximate the distance between the center of the core and the NH of the Ahx residue in **A-1** to a maximum value of ca. 18−19 Å. The corresponding value in **B-1** should be smaller by ca. 1.5 Å because of the smaller diameter of the 12-membered (β^3-HLys)$_3$ core structure.[41,44]

To investigate how the length and the nature of the linker can modulate the activity of CD40L mimetics, we have prepared a series of **B-1** variants (Chart 3) with oligomethylene [−$(CH_2)_n$−] tethers of length varying from $n = 3$ to 7 (Chart 3).

Chart 3

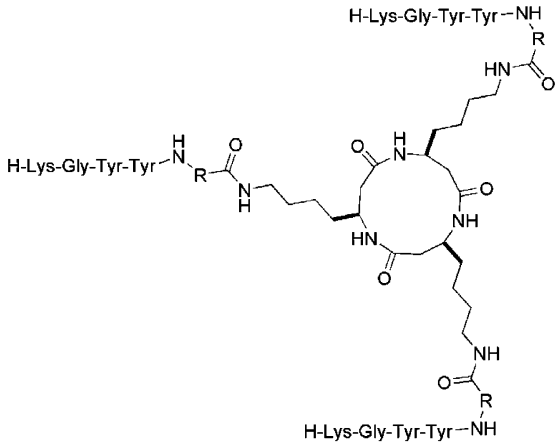

B-2 R = $(CH_2)_3$ (spacer Abu) **B-5** R = $(CH_2)_7$ (spacer Aoc)
B-3 R = $(CH_2)_4$ (spacer Apa) **B-6** R = $(CH_2)_{10}$ (spacer Aud)
B-1 R = $(CH_2)_5$ (spacer Ahx) **B-7** R = $[(CH_2CH_2O]_2$-CH_2 (spacer Ado)
B-4 R = $(CH_2)_6$ (spacer Ahp) **B-8** R = $[(CH_2CH_2O]_4$-CH_2 (spacer Ato)

Compound **B-2**, in which the oligomethylene chain is reduced by two carbons ($n = 3$), is no longer able to induce apoptosis of human B lymphoma BL41 cells (Figure 7a) and exhibits drastically reduced binding to CD40 (Figure 7b). Significant binding to CD40 is retained when the length of the spacer is decreased by only one carbon (**B-3**), although its association rate is lower than that for **B-1** (Figure 7b), but the capacity to induce apoptosis is not restored (Figures 7a and S5 for an annexin V−propidium iodide colabeling analysis). In contrast, analogues of **B-1** with one and two additional methylene groups (**B-4**, $n = 6$, and **B-5**, $n = 7$, respectively) induced significantly higher levels of apoptosis compared to **B-1** (Figures 7a and S5). The finding that the level of apoptosis is considerably enhanced as the spacer length increased from a three- to an optimal six-carbon chain, and remains constant upon an additional increment in chain length from $n = 6$ to $n = 7$, is consistent with other studies.[45,46] It has been shown previously, that in the case of flexible tethers, the effective molarity and potency are the highest for an optimal length and are only moderately affected by increments in chain length beyond this value.[41] Unfortunately, aggregation of **B-4** and **B-5** under SPR conditions precluded their evaluation for binding to CD40. Further increments in chain length from the 7-carbon chain to the 10-carbon chain led to a compound (**B-6**) with even lower solubility that could not be evaluated in the two assays. To increase the water solubility of the ligands, we also explored modification of the spacer by

(43) Kasai, N.; Yamanaka, T.; Miki, K.; Tanaka, N.; Post, B.; Morawetz, H. *Acta Crystallogr., Sect. B* **1981**, *37*, 1628−1630.

(44) The crystal structures of a number of isosteric cyclic tri(β-hydroxy alkanoates) have been solved. In crystal, these compounds generally adopt a flat, nearly equilateral triangular shape with all carbonyl groups pointing in one direction, very similar to the model calculated for *cyclo*-(β^3-HGlu)$_3$ (ref 36a) with a distance between the center of gravity of the triangle and the $^{\beta}$C ranging from 2.62 to 2.75 Å. See: (a) Seebach, D.; Muller, H.-M.; Burger, H. M.; Plattner, D. A. *Angew. Chem., Int. Ed. Engl.* **1992**, *31*, 434. (b) Seebach, D.; Hoffmann, T.; Kuhnle, F. N. M.; Lengweiler, U. D. *Helv. Chim. Acta* **1994**, *77*, 2007−2034.

(45) Sridhar, J.; Wei, Z.-L.; Nowak, I.; Lewin, N. E.; Ayres, J. A.; Pearce, L. V.; Blumberg, P. M.; Kozikowski, A. P. *J. Med. Chem.* **2003**, *46*, 4196−4204.

(46) Krishnamurthy, V. M.; Semetey, V.; Bracher, P. J.; Shen, N.; Whitesides, G. M. *J. Am. Chem. Soc.* **2007**, *129*, 1312−1320.

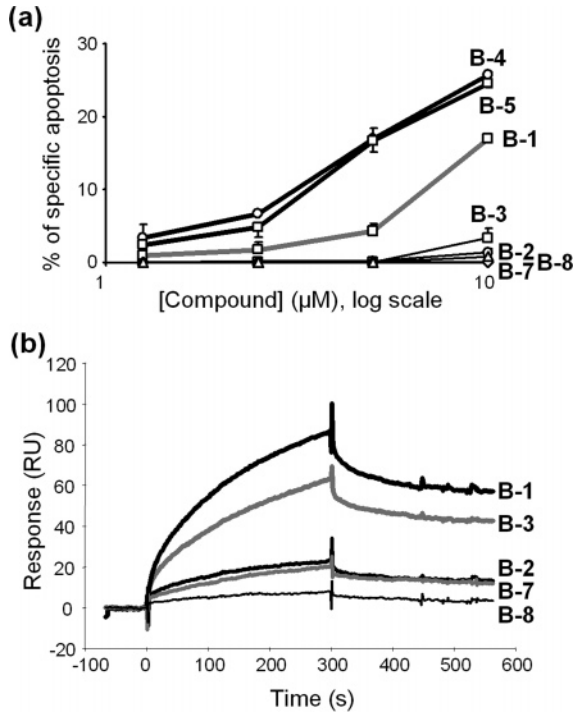

Figure 7. Influence of the length and nature of the linker. (a) Induction of apoptosis of human B lymphoma BL41 cells measured by reduction of $DiOC_6(3)$ dye uptake (see Experimental Section). Percentages of specific apoptosis induced by the different mimetics at the indicated concentrations after 16 h of incubation. Results are expressed as means ± SD of two independent experiments. (b) Direct binding to CD40 of **B-1** analogues at 200 nM as shown by SPR. Sensorgrams for **B-4** and **B-5** are not shown because of aggregation in the SPR conditions. All results are representative of at least two independent experiments.

substituting the saturated chain in **B-5** with a oligo(ethylene glycol) chain (EG_n) of similar length. This replacement resulted in a ligand (**B-7**) with dramatically reduced binding to CD40 and no apoptotic activity. No improvement was observed upon increasing further the number of oligo(ethylene glycol) units (e.g., **B-8**).

Overall the data obtained with the β-peptide core structure **B** suggest that *n*-amino-alkanoic acids as tethers are superior to corresponding oligoethylene glycol amino acids to distribute the CD40-binding motif and that a minimum carbon chain length (e.g., $n = 5-7$) is required to ensure binding to CD40 and effector functions. This result may partially explain why ligands such as **F-1** and **H-1** based on TREN and isocyanurate fail both in binding significantly to CD40 and in inducing apoptosis of B lymphoma cells. Even by assuming a fully extended conformation for the central core and the Ahx residue allowing a radial distribution of the CD40 binding motif, the distance between the center of the trimeric scaffold and the NH of the Ahx residue in **F-1** and **H-1** does not exceed 13 Å which is below the optimal 16 Å value.

The strong dichotomy observed between oligomethylene and oligo(ethylene glycol) tethers was not expected, and its origin remains unclear. Such a differential behavior has been documented previously in other systems including bivalent protein kinase C ligands[45] and might result from significant conformational differences and/or from a different propensity to interact with the surface of proteins.

***MiniCD40Ls* Based on Conformationally Restrained Receptor Binding Motifs.** To delineate the contribution to CD40

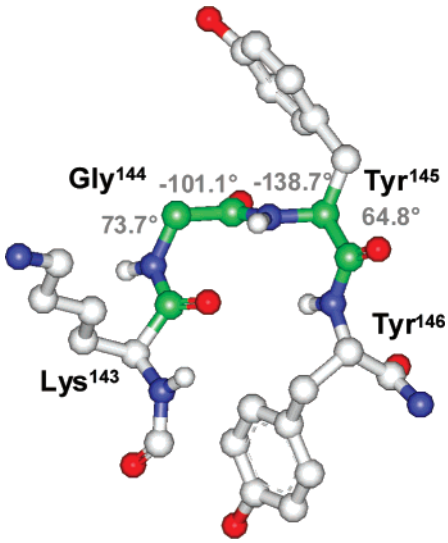

Figure 8. Reverse β-turn type conformation of the Lys^{143}-Gly-Tyr-Tyr^{146} CD40-binding motif in the crystal structure of CD40L.[24] The values of ϕ and ψ angles for residues $i+1$ (Gly^{144}) and $i+2$ (Tyr^{145}) are indicated.

Chart 4

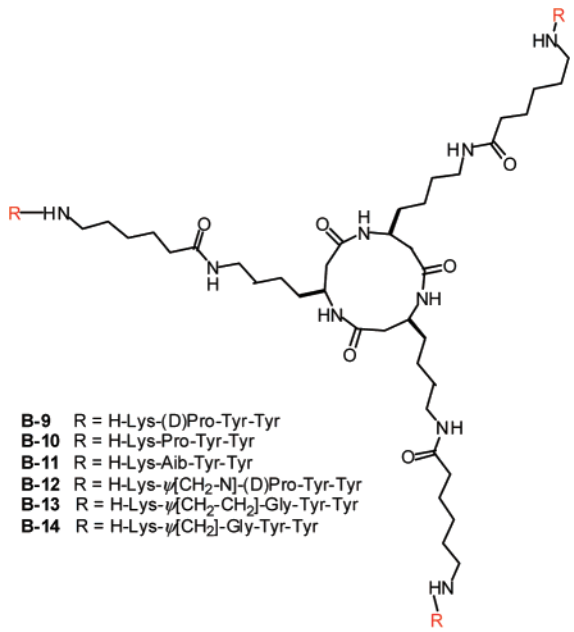

binding of each amino acid in the Lys-Gly-Tyr-Tyr sequence, we have previously prepared analogues of **B-1** singly substituted at each position by an alanyl (or glycyl) residue.[26a] We found that Lys and both Tyr residues are critical to binding and effector functions, consistent with data obtained from site-directed mutagenesis studies using recombinant CD40L molecules.[47] However, the glycyl residue is quite permissive and can be substituted by Ala without major decrease in binding to CD40 and with no strong reduction in the apoptotic activity on lymphoma cells.[26a] Examination of the geometry of the AA″ loop in the crystal structure of CD40L reveals that the four residues of the Lys-Gly-Tyr-Tyr CD40 binding motif located

(47) (a) Bajorath, J.; Chalupny, N. J.; Marken, J. S.; Siadak, A. W.; Skonier, J.; Gordon, M.; Hollenbaugh, D.; Noelle, R. J.; Ochs, H. D.; Aruffo, A. *Biochemistry* **1995**, *34*, 1833−1844. (b) Bajorath, J.; Marken, J. S.; Chalupny, N. J.; Spoon, T. L.; Siadak, A. W.; Gordon, M.; Noelle, R. J.; Hollenbaugh, D.; Aruffo, A. *Biochemistry* **1995**, *34*, 9884−9892.

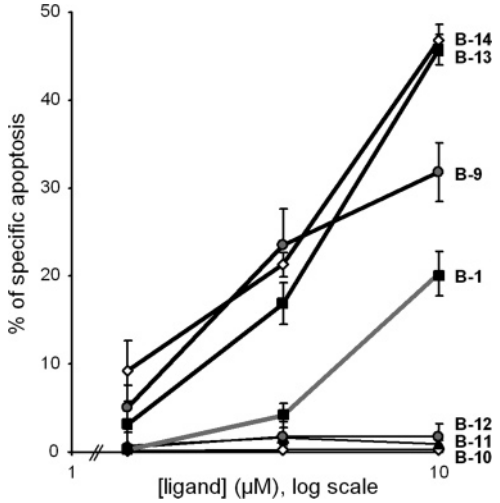

Figure 9. Induction of apoptosis of human B lymphoma BL41 cells by analogues of **B-1** containing modifications in the CD40-binding motif. Percentages of specific apoptosis are shown at the indicated concentrations after 16 h of incubation. Results are expressed as means ± SEM of three independent experiments.

at the top of the loop adopt a β-turn type conformation centered on Gly^{144} (i+1) and Tyr^{145} (i+2) residues. The corresponding backbone torsion angle values ϕ_{i+1}, ψ_{i+1}, and ϕ_{i+2} indicated in Figure 8 are close to values of an ideal reverse type-II′ β-turn [$\phi_{i+1} = +60°$ (±20°), $\psi_{i+1} = -120°$ (±20°), and $\phi_{i+2} = -80°$ (±20°)]. However, the precise conformation of the loop upon CD40 binding to CD40L remains to be elucidated.

To reduce the conformational space accessible to the glycyl residue and to approach the geometry of a reverse turn segment, we decided to introduce conformationally restricted amino acid residues such as D-Pro and Aib (α-amino isobutyric acid) which are known to facilitate β-turn conformations (Chart 4).[48] Whereas favored (ϕ,ψ) angles for D-Pro (+60°,+30° and +60°,−120°, respectively) are compatible with the requirements of the i+1 residue in both type-I′ and type-II′ β-turns, the (ϕ,ψ) space of Aib restricted to (+60°,+30°) and (−60°,−30°) values is compatible with type-I and type-I′ β-turns. Interestingly, substituting D-Pro for Gly (**B-1** → **B-9**) does not compromise binding to CD40 in SPR experiments. Analysis of kinetic data using the classical Langmuir monovalent model and local fittings revealed similar dissociation constants with K_D of 120 and 195 nM for **B-1** and **B-9**, respectively (see Supporting Information, Figure S6).[49] It is worth mentioning that the induction of apoptosis on human lymphoma cells was increased by this mutation, **B-9** being significantly more potent than **B-1** (Figure 9).

Preventing the possible formation of a reverse turn by substituting L-Pro for Gly (→ **B-10**) was detrimental for the apoptotic properties. Similarly, the insertion of an Aib residue at the i+1 position gave **B-11** which was not active on CD40 positive human lymphoma cells. Overall, these data give some hints about the bioactive conformation(s) of the Lys-Gly-Tyr-Tyr CD40-binding segment in *miniCD40Ls* and suggest

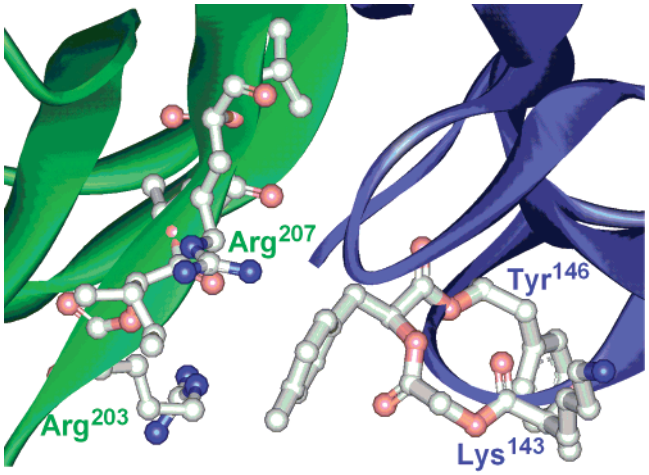

Figure 10. Part of the CD40 binding surface showing the relative positions of the putative CD40-binding sequences Lys^{143}-Gly-Tyr-Tyr^{146} (AA″ loop) and Arg^{203}-Leu-Leu-Ile-Arg^{207} (β-strand E) selected for the construction of first- and second-generation CD40L mimetics.

Scheme 3 [a]

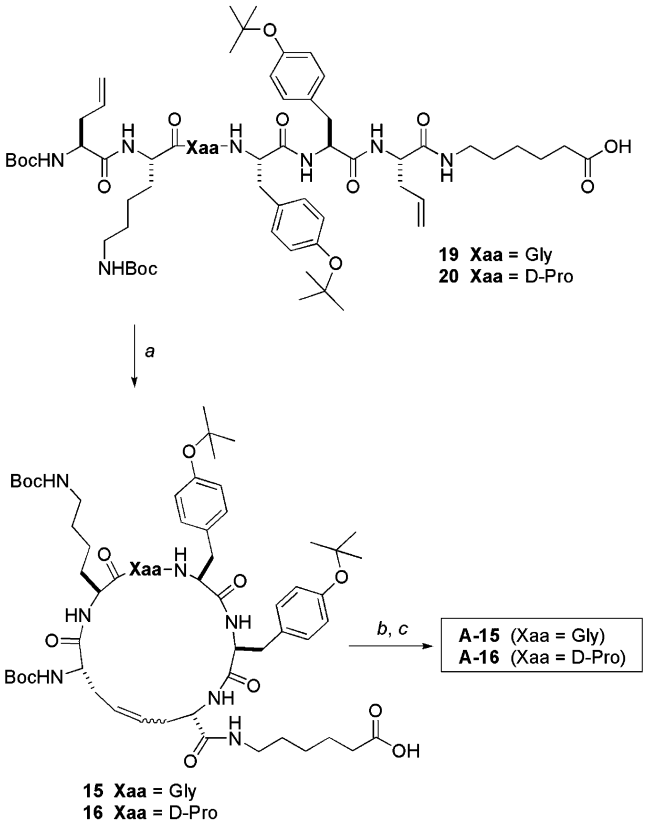

[a] Reagents and conditions: *a*: Grubbs catalyst II; CH_2Cl_2, 50 °C, 7 days; *b*: **A-0** (0.3 equiv), BOP, DIEA, DMF, 24 h; *c*: TFA/H_2O (95:5).

possibilities to further modulate/optimize effector functions of *miniCD40Ls* using appropriate modifications centered on the Gly residue. The insertion of pseudopeptide bonds between i and i+1 residues to create local conformational perturbations that could eventually modulate the effector functions of *miniCD40Ls* **B-1** and **B-9** was also evaluated (Chart 4). Whereas the introduction of a reduced peptide (methylene amino) bond [denoted $\psi(CH_2-N)$ according to Spatola's nomenclature for pseudopeptide bonds][50] was found to be detrimental for biological activity, analogues **B-13** and **B-14** with ethylene

(48) For reviews, see: (a) Venkatraman, J.; Shankaramma, S. C.; Balaram, P. *Chem. Rev.* **2001**, *101*, 3131−3152. (b) Rose, G. D.; Gierasch, L. M.; Smith, J. A. *Adv. Protein Chem.* **1985**, *37*, 1−110.

(49) It is noteworthy that similar results were obtained for analogous ligands **A-1** and **A-9** (ref 35). In this case, K_D calculated using the Langmuir 1:1 model and local fitting models were 121 and 183 nM, respectively. Analysis of cooperativity using Hill plots suggested that the **A-1**/CD40 interaction is cooperative (Hill coefficient $h = 2.9$) and that this cooperativity is lost upon replacing Gly by D-Pro ($h = 1.0$).

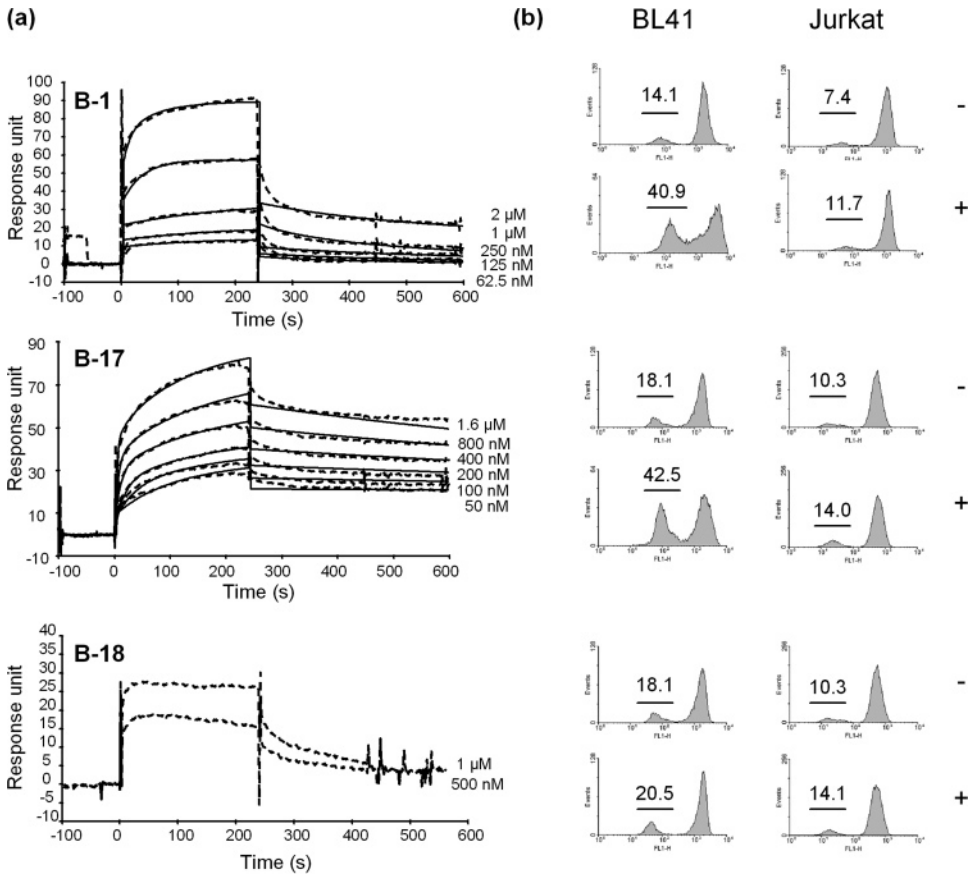

Figure 11. Comparison of *miniCD40Ls* with binding motifs derived from distinct CD40L hot-spot regions [e.g., Lys[143]-Gly-Tyr-Tyr[146] from the AA″ loop (**B-1**), Arg[203]-Leu-Leu-Ile-Arg[207] from β-strand E (**B-17**), and Gly[199]-Arg-Phe-Ile-Arg[203] from DE loop (**B-18**)]. (a) Direct binding to CD40 at different concentrations of mimetics as shown by SPR. Dashed lines represent experimental curves, straight lines represent fitting curves. All results are representative of at least two independent experiments. (b) Induction of apoptosis of human B lymphoma cells BL41 and Jurkat cells (human CD40-negative cells) after 16 h of incubation with 10 μM of the different mimetics (+) or in culture medium alone (−). Results are representative of three independent experiments. Percentage of apoptotic cells is shown above the apoptotic left-peak on each histogram.

$\psi(CH_2-CH_2)$ and methylene $\psi(CH_2)$ bonds were significantly more potent than **B-1** in inducing apoptosis of CD40 positive B lymphoma cells (Figure 9 and Figure S5). Noteworthy, using the trivalent model, **B-14** was found to bind CD40 with an overall K_D of 2.8 nM calculated using the trivalent model with local fitting (the Langmuir 1:1 model gave poor fitting, see Supporting Information, Figure S7). The substitution of a ψ-(CH_2) methylene linkage for the amide bond between Lys and Gly consists in the replacement of the Lys-Gly segment by a γ^4-Lys residue. Similarly, substitution of γ-amino acid for α-amino acid residues in the central type-II′ β-turn forming tetrapeptide fragment of octreotide, a potent analogue of somatostatin, led to the discovery of open-chain peptidomimetics with nanomolar affinities for certain human somatostatin receptor subtypes.[51]

Alternatively, the conformational space accessible to the linear receptor binding peptide can be dramatically reduced through cyclization. Ring-closing methatesis of fully protected linear hexapeptides **17** and **18** containing Lys-Gly-Tyr-Tyr and Lys-D-Pro-Tyr-Tyr epitopes and a free carboxylic acid tail, using Grubbs catalyst,[52] afforded cyclopeptides **15** and **16** ready for coupling onto triamine cores. The corresponding ligands **A-15** and **A-16** with cyclic CD40 binding segments were synthesized and purified according to our general procedure and evaluated for binding to recombinant human CD40 by SPR and for effector functions (see Scheme 3). Although binding to CD40 was observed in direct SPR experiments (see Supporting Information, Figure S8),[53] **A-15** and **A-16** turned out to be inactive in the apoptotic assay (see Supporting Information, Figure S9). One can speculate that the loss of activity observed is associated with unwanted conformational changes and low population of a type-II′ β-turn conformation. Alternatively, the readily accessible and recently reinvestigated DL_4 cyclopentapeptide template could be used to enforce type-II′ β-turn conformation with the D-amino acid residue at the $i+1$ position.[54]

Second-Generation Mimetics Based on a New CD40-Binding Motif. Molecular modeling experiments and X-ray crystal data indicate that the surface area buried upon complexation of CD40L and CD40 is ca. 850 Å^2 and is highly polar.[25] Residues of CD40L in contact with CD40 are distributed over two CD40L molecules. Although the Lys-Gly-Tyr-Tyr loop

(50) Spatola, A. F. In *Chemistry and Biochemistry of Amino Acids, Peptides and Proteins*; Weinstein, B., Ed.; Marcel Dekker Inc.: New York, 1983; Vol. 7, pp 267−357.
(51) Seebach, D; Schaeffer, L.; Brenner, M.; Hoyer, D. *Angew. Chem., Int. Ed.* **2003**, *42*, 776−778.
(52) Scholl, M.; Ding, S.; Lee, C. W.; Grubbs, R. H. *Org. Lett.* **1999**, *1*, 953−956.
(53) In the case of **B-15**, fitting of SPR data was better achieved with divalent and trivalent models (χ^2 = 0.271 and 0.269, respectively) than with the "Langmuir 1:1" monovalent model (χ^2 = 0.843).
(54) (a) Mierke, D. F.; Kurz, M.; Kessler, H. *J. Am. Chem. Soc.* **1994**, *116*, 1042−1049. (b) Heller, M.; Sukopp, M.; Tsomaia, N.; John, M.; Mierke, D. F.; Reif, B.; Kessler, H. *J. Am. Chem. Soc.* **2006**, *128*, 13806−13814.

motif from one subunit is critical for CD40L binding to CD40, site-directed mutagenesis studies have identified another hot-spot region located on β-strand E and encompassing residues Arg^{203} and Arg^{207} (Figure 10).

It has been suggested from site-directed mutagenesis experiments and calculations that these positively charged side-chains (Lys^{143}, Arg^{203}, and Arg^{207}) can make contacts with oppositely charged residues on CD40, namely Glu^{66}, Glu^{74}, Asp^{84}, and Glu^{117} and that the resulting CD40−CD40L charged pairs Arg^{203}-Glu^{74}, Arg^{207}-Asp^{84}, Arg^{207}-Glu^{117} have a net stabilizing effect on the complex. On the basis of distance considerations, calculation of desolvation energy and total electrostatic stabilization, the Arg^{203}-Glu^{74} pair (3.2 Å) was proposed to be the strongest salt bridge in the model. These data thus suggested to us that other sequences, derived from the second symmetry related subunit or combinations of sequences could in principle be used to design second generation CD40L mimetics. Two linear pentapeptide sequences mapping residues Gly^{199} to Arg^{207} on loop DE and β-strand E and containing Arg^{203} (N− or C-terminal) were considered as possible CD40 binding units. The corresponding trimeric architectures were assembled on β-tripeptide core **B** with an Ahx linker and compared directly to *miniCD40L* **B-1** in SPR and cellular assays. The results are reported in Figure 11.

SPR measurements at different concentrations (Figure 11a) showed that compound **B-17** (R = H-Arg-Leu-Leu-Ile-Arg), but not **B-18** (R = H-Gly-Arg-Phe-Ile-Arg), binds significantly to CD40. Analysis of kinetic data using the Langmuir 1:1 model and local fitting gave an mean K_D of 4.4 nM for **B-17** (vs 120 nM for **B-1**). Like for **B-1**, local fitting using a trivalent model gave lower χ^2 values (0.54 versus 7.5 for the langmuir 1:1 model and 2:1 for the divalent model), suggesting binding in a trivalent manner. Interestingly, **B-17** was also found to be as potent as **B-1** in inducing apoptosis of human lymphoma B cells (42.5% apoptosis versus 40.9% at 10 μM after 16 h of treatment, Figure 11b). Preliminary data also indicate that **B-17** like **B-1** is effective in inducing the maturation of the D1 dendritic cell line (data not shown). Overall, these biochemical and biological data underscore further the versatility of rigid and planar α- and β-cyclopeptide based scaffolds **A** and **B** for the design of *miniCD40Ls*.

Conclusion

Molecules with multiple copies of a recognition motif appended to a central scaffold have unique properties that differ from those of monovalent compounds. In particular, designed multivalent systems can mediate cell-surface receptor oligomerization and display effector functions.[14] *MiniCD40Ls* are relatively small (<3 kDa), rationally designed synthetic multimeric architectures that mimic, both in vitro[26] and in vivo[28] the effects of CD40L, a noncovalent homotrimeric protein belonging to the TNF superfamily. Because they are chemically defined and tunable, synthetic multivalent ligands are very attractive molecules to delineate molecular determinants of effector functions and to control receptor assembly in signal transduction.[14] Our data are consistent with C_3-symmetry and radial distribution of the CD40-binding motif being two essential features leading to mimetics with effector functions. The distance between the center of the scaffold and the binding moiety is also a critical element of the design. Flat cyclic peptides of 5−8 Å diameter (e.g., **A** and **B**) with side arms linked to flexible oligomethylene spacers are very versatile systems for trivalent display of CD40-binding motifs.[55] For example, *miniCD40Ls* **B-1** and **B-17** which utilize distinct CD40-binding elements, namely Lys^{143}-Tyr^{146} on loop AA″ and Arg^{203}-Arg^{207} on β-strand E have the same trimeric scaffold−linker combination $(Ahx)_3$-**B**. Examination of the crystal structure of homotrimeric CD40L[24] shows, however, that the two equilateral triangles whose vertices are formed by the three α-amino groups of the residue immediately following Tyr^{146} and Arg^{207} (Thr^{147} and Ala^{208}, respectively) largely differ in size, with centroid-to-vertex distances of ca. 16 and 10 Å, respectively (Figure 12).

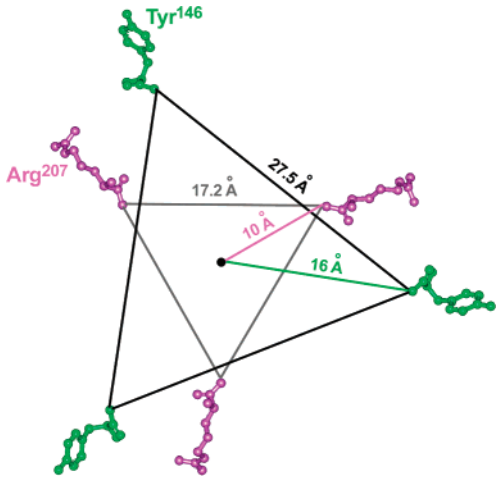

Figure 12. Schematic representation of the two equilateral triangles whose vertices are formed by α-amino groups of residues immediately following Tyr^{146} (green) and Arg^{207} (pink) according to the X-ray crystal coordinates of homotrimeric CD40L.[24] Distances from centroid to vertex are indicated.

Although this observation underscores the versatility of the $(Ahx)_3$-**B** system, it also suggests that a scaffold−linker combination consisting of a shorter linker or a smaller scaffold (e.g., heterocyclic) could be considered in principle to tether the Arg^{203}-Arg^{207} binding moiety.

All TNF superfamily members share the same overall topology and are active as homotrimers. Thus, one can conceive that a general approach based on the use of peptide templates **A** and **B** could be transposable to other TNF family members. While this work was in progress, researchers at Genentech and Affymax, independently reported peptide sequences that specifically bind to the human DR5 (hDR5), one of the signaling receptors for TNF-related apoptosis-inducing ligand (TRAIL).[56] Interestingly, oligomeric forms were generated either by fusion of these peptides to leucine zipper variants[57] that form either dimers, trimers, or tetramers[56a] or simply by dimerization.[56b] Avidity to hDR5 was significantly improved through oligomerization of DR5-binding peptides and some of these multimeric

(55) For selected examples of polyvalent systems based on cyclic peptide templates of different topology, see: (a) Singh, Y.; Dolphin, G. T.; Razkin, J.; Dumy, P. *ChemBioChem* **2006**, *7*, 1298−1314. (b) Reference 10e. (c) Zhang, Z.; Liu, J.; Verlinde, C. L. M. J.; Hol, W. G. J.; Fan, E. *J. Org. Chem.* **2004**, *69*, 7737−7740.

(56) (a) Li, B.; Russell, S. J.; Compaan, D. M.; Totpal, K.; Marsters, S. A.; Ashkenazi, A.; Cochran, A. G.; Hymowitz, S. G.; Sidhu, S. S. *J. Mol. Biol.* **2006**, *361*, 522−36. (b) Angell, Y. M.; et al. In *Understanding Biology Using Peptides*; Blondelle, S. E., Ed.; Proceedings of the Nineteenth American Peptide Symposium, Series: American Peptide Symposia, Vol. 9; Springer: New York, 2006; pp 405−406.

(57) Harbury, P. B.; Zhang, T.; Kim, P. S.; Alber, T. *Science*, **1993**, *262*, 1401−1407.

constructions were found to display significant cytotoxic activity. These results which confirm that peptide scaffolding on multivalent core structures is a viable approach to generate *miniTNFs*, also expand the set of eligible multimeric architectures. It is worth mentioning that self-organization into noncovalent homotrimers with C_3-symmetry axis is not limited to TNF family members and is also a structural feature of proteins such as TNF-receptor-associated factor (TRAF),[58] collectins [e.g., mannan binding lectins (MBLs), surfactant proteins SP-A and SP−D],[59] members of the C1q family,[60] adenovirus fiber head (knob domain) emanating from the vertices of the icosahedral capsid,[61] or envelope (Env) glycoproteins of HIV type-1 (HIV-1).[62] It remains to be seen whether these protein trimers could also be mimicked (or targeted) with trimeric architectures such as those reported here.[63]

By signaling through CD40, CD40L plays an active role in a variety of immune responses, allowing B cells to differentiate, proliferate, and isotype class switch, activating antigen presenting cells (e.g., dendritic cells) and mediating T-cell help for cytotoxic T lymphocytes. Therefore, small molecule CD40L mimetics could be potentially useful as immunopotentiators. TNF family ligands are type-II transmembrane proteins with an extracellular, homotrimeric C-terminal TNF homology domain that is frequently released as a soluble cytokine upon proteolytic processing. However, receptor trimerization of TNF-R superfamily members by their soluble ligands is not always sufficient to reach the activation threshold. In particular, full activation of CD40 which leads to B-cell proliferation and isotype switching requires higher-order receptor oligomerization. This is typically achieved not only by membrane-bound CD40L but also by cross-linking with antibodies or by using artificial fusion proteins consisting of multiple copies (two or four) of CD40L trimers.[64] By analogy, it is tempting to speculate that similar synergistic effects could be generated through multivalent display of *miniCD40Ls*. CD40L mimetics disclosed in this work together with their higher-order multimeric versions would certainly constitute a unique set of probes to investigate the relationship between receptor oligomerization and cell signal transduction. This possibility will be addressed in future extension of this work.

Experimental Section

Synthesis of Ligands. See Supporting Information.

Biological Reagents. Recombinant soluble human CD40-mouse Ig fusion protein (rshCD40:mIg) and recombinant soluble human CD40L coupled to the mouse CD8-α extracellular domain (rshCD40L:mCD8) were purchased from Ancell corporation (Bayport, MN). Surfactant P20 was purchased from Biacore AB (Uppsala, Sweden). The 3,3′-dihexyloxacarbocyanine iodide $DiOC_6(3)$ dye was purchased from Interchim (Montluçon, France). Fluorescein isothiocyanate (FITC)-conjugated anti-mouse CD40 (3/23 clone), FITC anti-human CD40 (5C3 clone), phycoerythrin (PE) anti-mouse CD54 (3E2 clone), PE anti-mouse CD80 (16-10A1 clone), and PE anti-mouse CD86 (GL1 clone) mAbs were purchased from Pharmingen (San Jose, CA). Low endotoxin recombinant mouse granulocyte/macrophage colony stimulating factor (rmGM-CSF) was purchased from USBiological (Swampscott, MA).

Surface Plasmon Resonance Analysis. BIAcore 3000 (Biacore AB) was used to evaluate the binding of CD40L mimetics to CD40. Flow cells of a CM5 sensor chip (Research Grade, Biacore AB) were precoated with rabbit polyclonal antibodies directed against mouse immunoglobulin (Ig) domain (RAM-Ig, Biacore AB) using amine coupling at 30 μg/mL in 10 mM acetate buffer, pH 5.5 according to the manufacturer's instructions. The chip was then flushed with 1 M ethanolamine hydrochloride pH 8.5 (Biacore AB) and 50 mM HCl to eliminate unbound antibody. Generally ca. 10,000 response units (RU), corresponding to 10 ng/mm^2, of RAM-Ig were immobilized. Biosensor assays were performed at 25 °C with HBS-EP buffer [10 mM HEPES (pH 7.4), containing 0.15 M NaCl, 3.4 mM EDTA, and 0.005% v/v surfactant P20] as running buffer. Capture of rshCD40:mIg and of LG11-2, a mouse IgG2a mAb directed against H2B histone used as irrelevant control (purified by protein G affinity chromatography from hybridoma supernatant), was performed on individual flow cells at a flow rate of 5 μL/min and at a concentration that would achieve equivalent protein mass binding. A small amount of protein was captured, ca. 450 RU, sufficient for the detection of the binding of the CD40 ligands, and limiting the mass transport and rebinding artefacts.

CD40L mimetics and rshCD40L:mCD8 were then injected (kinetic mode) at a flow rate of 30 μL/min over the control and CD40 channels for 4 min and allowed to dissociate for an additional 3 min. The flow cells were regenerated for 30 s with 50 mM HCl. A 1-Hz acquisition mode was sufficient for subsequent good assessment of kinetic constants. Control sensorgrams were subtracted from the CD40 ones and analyzed by BIAevaluation 4.1 with various models.

The simplest "Langmuir 1:1" model was first used to assess the binding kinetics of the interaction. A complete description of equations used for kinetics data determination can be found in the Biacore AB Handbook and is summarized in Supporting Information. The trivalent analyte model was also used to evaluate the stoichiometry and to get some details on the mechanism of the binding, in particular the distinct rates for all binding and conformational change events, but due to complexity of the equations and the limited integrative possibilities offered by the BIAevaluation software, cooperativity was assessed with the R_{eq} values (from a trivalent model with freedom in the determination of the association and dissociation rate constants of the first interaction) and the R_{max} value as well as all other rate constants globally processed for the sets of concentrations of the CD40-ligands.

Accuracy of the fits was measured by the *Chi square* (χ^2) value, which evaluates the deviation of the fitted model from the experimental points. Residuals were also shown to give better insight into whether a model is accurate, as the bandwidth and its shape reveal the differences between the fitted curve and the experimental data.

Surface Plasmon Resonance Analysis: Summary of the Equations Used for the Determination of the Kinetics Data. The simplest model, the Langmuir 1:1 one, was first used to assess the binding kinetics of the interaction. In the following equations, L denotes the ligand captured on the immobilized rabbit anti-mouse Ig, in our case the receptor CD40, and A denotes the analyte injected on the chip, that is either of the CD40L or *miniCD40Ls*. When A interacts with L forming the LA complex due to diffusion, collision, and binding, in function of time with the association rate constant k_a (M^{-1} s^{-1}), but can also disappear with dissociation rate constant k_d (1/s) to release A from L (eq 1).

(58) McWhirter, S. M.; Pullen, S. S.; Holton, J. M.; Crute, J. J.; Kehry, M. R.; Alber, T. *Proc. Natl. Acad. Sci. U.S.A.* **1999**, *96*, 8408−8413.
(59) Hakansson, K.; Reid, K. B. *Protein Sci.* **2000**, *9*, 1607−1617.
(60) Kishore, U.; Gaboriaud, C.; Waters, P.; Shrive, A. K.; Greenhough, T. J.; Reid, K. B.; Sim, R. B.; Arlaud, G. J. *Trends Immunol.* **2004**, *25*, 551−561.
(61) Bewley, M. C.; Springer, K.; Zhang, Y. B.; Freimuth, P.; Flanagan, J. M. *Science* **1999**, *286*, 1579−1583.
(62) Zhu, P.; Liu, J.; Bess, J., Jr.; Chertova, E.; Lifson, J. D.; Grise, H.; Ofek, G. A.; Taylor, K. A.; Roux, K. H. *Nature* **2006**, *441*, 847−852.
(63) Synthetic trivalent miniproteins designed to target the CD_4-binding sites on the HIV-1 Env glycoprotein gp120 trimers have been reported recently. Li, H.; Guan, Y.; Szczepanska, A.; Moreno-Vargas, A. J.; Carmona, A. T.; Robina, I.; Lewis, G. K.; Wang, L. X. *Bioorg. Med. Chem.* **2007**, *15*, 4220−4228.
(64) Holler, N.; Tardivel, A.; Kovacsovics-Bankowski, M.; Hertig, S.; Gaide, O.; Martinon, F.; Tinel, A.; Deperthes, D.; Calderara, S.; Schulthess, T.; Engel, J.; Schneider, P.; Tschopp, J. *Mol. Cell. Biol.* **2003**, *23*, 1428−1440.

$$L + A \underset{\leftarrow k_d}{\overset{k_a \rightarrow}{\rightleftharpoons}} LA \quad (1)$$

Equilibrium is reached when the rate of association (eq 2) equals the rate of dissociation, that is when the number of dissociation events compensates the number of association events.

$$\frac{d[LA]}{dt} = k_a[L][A] - k_d[LA] \quad (2)$$

Under our conditions, equilibrium cannot be reached at the end of the injection phase, but values at equilibrium could be extrapolated, especially the dissociation constant K_D (M), using the kinetic values obtained from the individual experimental curves of the association and dissociation phases (eq 3).

$$\frac{[L][A]}{[LA]} = \frac{k_d}{k_a} = K_D \quad (3)$$

Rewriting eq 2 in terms of concentration and responses, we obtain eq 4.

$$\frac{dR}{dt} = k_a C(R_{max} - R_t) - k_d R_t \quad (4)$$

In eq 4, R_t corresponds to the response signal of the formed complex at t time, C represents the concentration of CD40-ligands, and R_{max} is the maximal feasible response signal, depending on the total CD40-binding capacity (or activity) on the sensor chip. In this case we assume that free ligand equals maximal capacity minus bound receptor.

The data extracted from the experimental curves as well as the known input parameters are used by the algorithm and assessed by numerical integration to calculate the different parameters needed. One can then determine the values for signal response at equilibrium (R_{eq}), that is for t value tending to infinite, from the kinetic constants and the R_{max} calculated parameter (eq 5).

$$R_{eq} = \frac{k_a Conc \times R_{max}}{k_a Conc + k_d} \quad (5)$$

Culture of Lymphoma Cells and Measurement of Apoptosis. BL41 Burkitt lymphoma and Jurkat human T leukemia cells were cultured in RPMI 1640 (Cambrex Bioscience, Verviers, Belgium) supplemented with 10% of heat-decomplemented fetal bovine serum (FBS; Dominique Dutscher, Brumath, France) and gentamicin (10 μg/mL, Cambrex). For apoptosis assays, cells (5×10^5 cells/mL) were incubated at 37 °C in flat-bottom 96-well plates at the indicated times and concentrations in the presence of various *miniCD40Ls* in 200 μL of complete medium. After incubation, cells were washed with phosphate-buffered saline (PBS), and apoptosis was evaluated by measurement of a decrease in mitochondrial transmembrane potential ($\Delta\psi_m$) associated with a reduction of the cationic dye $DiOC_6(3)$ uptake, as detected by flow cytometry. For this, cells were resuspended in 300 μL of PBS containing 20 nM of $DiOC_6(3)$, incubated at 37 °C for 20 min, and then directly analyzed by flow cytometry.

Results are expressed as the percentage of specific apoptosis according to the following formula:

$$\% \text{ of specific apoptosis} = \frac{100\ (\% \text{ apoptotic treated cells} - \% \text{ spontaneous apoptotic control cells})}{(100 - \% \text{ spontaneous apoptotic control cells})}$$

Culture and Maturation of D1 Mouse Dendritic Cell Line. D1 cells have been described as a MHC class II-positive growth factor-dependent immature dendritic cells, derived from adult mouse spleen maintained in lineage without being transformed.[30] Cells were cultured in nontreated plastic dishes IMDM with HEPES and L-glutamine (Cambrex), supplemented with 10% of heat-decomplemented FBS, gentamicin (10 μg/mL), 10 μM β-mercaptoethanol, and 10 ng/mL of rmGM-CSF. For cellular assays, 2×10^5 cells/mL were cultured for 24 h in 24-well untreated polystyrene microplates (Evergreen Scientific, Los Angeles, CA). Then, fresh medium containing the various *miniCD40Ls* was added. After an additional 24 h of incubation, cells were washed with cold PBS and harvested with 2 mL of PBS containing 2 mM EDTA. After centrifugation, cells were resuspended in cold PBS and analyzed for cell surface phenotyping by flow cytometry.

Flow Cytometry Analysis. For measurement of apoptosis, lymphoma cells were analyzed directly after the staining procedure. For phenotyping, D1 cells were stained in PBS containing 2% FBS at 4 °C for 20 min with the various antibodies used at concentrations recommended by the manufacturer. After two washes in PBS, cells were analyzed by flow cytometry with a FACSCalibur. At least 1×10^5 events were acquired for each experiment using CellQuest version 3.3 (Becton Dickinson, Pont de Claix, France), and the data were processed with WinMDI, version 2.8 freeware (Joseph Trotter, Scripps Research Institute, http://facs.scripps.edu/software.html).

Acknowledgment. We thank J. P. Briand and S. Muller for their continuous support. This work was supported by the CNRS, the Ministère de la Recherche (ACI "Jeunes Chercheurs"), "La Ligue contre le Cancer" and INCA (Cancer: détection d'innovations 2006, #50). W.S. and S.W. were supported by grants from the Ministère de la Recherche and from the Fondation pour la Recherche Médicale (FRM). N.T. was supported by "La Ligue contre le Cancer". We thank N. Bonnefoy-Berard and M. Flacher for providing the lymphoma cells, C. J. M. Melief for providing the dendritic cell line D1, M. Monestier for providing the LG11-2 hybridoma. We acknowledge O. Reinaud for a generous gift of calix[6]triamine **D-0**.

Supporting Information Available: Detailed procedures and characterization data of all ligands as well as additional surface plasmon resonance (SPR) sensorgrams and analysis; complete refs 21b and 56b. This material is available free of charge via the Internet at http://pubs.acs.org.

JA073169M